A novel, structure-preserving, second-order-in-time relaxation scheme for Schrödinger-Poisson systems

Athanassoulis, Agissilaos; Katsaounis, Theodoros ; Kyza, Irene; Metcalfe, Stephen

DOI:
10.48550/arXiv.2103.04903

Publication date:
2022

A NOVEL, STRUCTURE-PRESERVING, SECOND-ORDER-IN-TIME RELAXATION SCHEME FOR SCHRÖDINGER-POISSON SYSTEMS

AGISSILAOS ATHANASSOULIS, THEODOROS KATSAOUNIS, IRENE KYZA, AND STEPHEN METCALFE

Abstract. We introduce a new structure preserving, second order in time relaxation-type scheme for approximating solutions of the Schrödinger-Poisson system. More specifically, we use the Crank-Nicolson scheme as a time stepping mechanism, whilst the nonlinearity is handled by means of a relaxation approach in the spirit of [10, 34] for the nonlinear Schrödinger equation. For the spatial discretisation we use the standard conforming finite element scheme. The resulting scheme is explicit with respect to the nonlinearity, i.e. it requires the solution of a linear system for each time-step, and satisfies discrete versions of the system's mass conservation and energy balance laws for constant meshes. The scheme is seen to be second order in time. We conclude by presenting some numerical experiments, including an example from cosmology and an example with variable time-steps which demonstrate the effectiveness and robustness of the new scheme.

1. Introduction

1.1. **Statement of the problem.** Schrödinger-Poisson-type systems appear in many applications, including semiconductors [40, 31, 38], plasma physics [15, 41], optics [39] and cosmology [44, 35, 45, 21]. In this paper we consider a class of Schrödinger-Poisson systems (SPS), namely the following initial-boundary value problem, either with homogeneous Dirichlet boundary conditions or periodic boundary conditions: We seek a *wavefunction* $u : \Omega\times(\tau,T) \to \mathbb{C}$ and the associated *potential* $\mathsf{v} : \Omega\times(\tau,T) \to \mathbb{R}$ such that

$$
\begin{cases}
u_t - \mathrm{i}p(t)\Delta u + \mathrm{i}q(t)\mathsf{v}u = 0, & \text{in } \Omega\times(\tau,T),\\
\Delta\mathsf{v} = |u|^2 - \mu, & \text{in } \Omega\times(\tau,T),\\
u(\mathbf{x},\tau) = u_0(\mathbf{x}), & \text{in } \Omega,\\
\{\mu = 0 \text{ and } u = \mathsf{v} = 0\}, \quad \text{OR} \quad \{\mu = \|u_0\|_{L^2}^2 \text{ and } u, \mathsf{v} \text{ periodic,}\} & \text{on } \partial\Omega\times(\tau,T],
\end{cases}
\tag{1.1}
$$

In (1.1), $\tau \geq 0$ is a given initial time and $T > \tau$ is a given final time. The domain $\Omega \subset \mathbb{R}^d$, $d = 1, 2, 3$, is assumed to be bounded, convex and polygonal in the Dirichlet case, and a $d-$dimensional parallelepiped in the periodic case. The normalisation of μ ensures that the elliptic problem is well-posed in both cases. For the initial condition we have $u_0 \in H^1(\Omega)$. The coefficients $p(t)$, $q(t)$ are smooth and real valued; the introduction of time-dependent coefficients is directly motivated by the cosmological application [44, 35]. More details and simulations of that problem can be found in Section 5.4.

System (1.1) satisfies mass conservation and energy balance laws that are of great physical relevance. These are discussed in detail in Section 2. Proposing schemes that satisfy discrete analogues of these laws is a significant goal, as typically this leads to good qualitative behaviour of numerical solutions for longer computational times. Moreover, when these discrete laws are verified unconditionally in the time-step size, this provides flexibility for dealing with stiffness issues. Structure preserving schemes for (1.1) are of great physical relevance since in recent years the SPS system is used extensively as an alternative to the computationally expensive Vlassov-Poisson system with applications in cosmology, see e.g. [35, 44, 45] and the references therein.

Our goal in this paper is to propose a scheme that is is linearly implicit, unconditionally structure preserving (in the sense of satisfying discrete energy and mass balance laws without restriction

Date: December 23, 2022.

Key words and phrases. Schrödinger-Poisson system, Relaxation scheme in time, Crank-Nicolson method, finite element method.

on the time-step size) and second order accurate in time. An important advantage of linearly implicit schemes is that they are faster. Moreover, they are easier to implement, as no iterative scheme (Newton, fixed point etc) has to be selected and calibrated. Finally, by being more directly implementable, linearly implicit schemes are more amenable to further work on a posteriori error control.

An important special case of (1.1) is the problem with constant coefficients and homogeneous Dirichlet boundary conditions; taking $p(t) = \dfrac{\varepsilon}{2\alpha^2}$, $q(t) = \dfrac{\beta}{\varepsilon\alpha}$ and $\mu = 0$ we obtain the following standard Schrödinger-Poisson system,

$$\begin{cases} u_t - \dfrac{i\varepsilon}{2\alpha^2}\Delta u + \dfrac{i\beta}{\varepsilon\alpha}\mathsf{v}u = 0, & \text{in } \Omega\times(\tau,T), \\ \Delta\mathsf{v} = |u|^2, & \text{in } \Omega\times(\tau,T), \\ u = 0,\ \mathsf{v} = 0, & \text{on } \partial\Omega\times(\tau,T], \\ u(\mathbf{x},\tau) = u_0(\mathbf{x}), & \text{in } \Omega, \end{cases} \tag{1.2}$$

where the parameter ε represents the ratio of the Planck constant to the mass of the particle, while $\alpha > 0$ and $\beta \in \mathbb{R}$ are given constants. When ε is small, this is called the semiclassically scaled problem, and it is expected formally that as $\varepsilon \to 0^+$ the Schrödinger-Poisson system (1.2) approximates, in some sense, the classical Vlasov-Poisson equations, cf., e.g., [48].

Concerning the existence and uniqueness of solutions to the Schrödinger-Poisson system (1.2), most of the analytical results are for the full space case $\Omega = \mathbb{R}^d$; we refer to the works [17, 18, 29] and the book [19]. In [1], the authors analyze a transient Schrödinger-Poisson system with transparent boundary conditions while in [43] the stationary spherically symmetric case was analyzed. The asymptotic behaviour of solutions to the Schrödinger-Poisson system is studied in [5] via a variational approach.

1.2. **Existing numerical methods for the Schrödinger-Poisson system.** There exists a very large literature for the numerical approximation of the nonlinear Schrödinger equation with power nonlinearity (NLS), cf. e.g. [10, 11, 34, 4, 2, 3, 26, 22, 7, 32, 33, 14, 20, 23, 24, 28, 12, 27, 42, 49] and the references therein for a sample of such works. In contrast, the numerical methods available for the SPS are not that many. In what follows, we focus on numerical methods for the SPS (1.1).

The existing methods in the literature for SPS are with uniform temporal and mesh sizes and/or the nonlinear term is treated implicitly. This leads to practical difficulties, which might be the reason that in the literature most of the numerical implementations for the SPS (1.1) are performed in the one-dimensional case.

More precisely, popular methods in the literature for the approximation of the SPS (1.1), include the Crank-Nicolson, the Gaussian beam or the time-splitting method for the time-discretization, while finite differences or spectral methods are used for the spatial discretization. In [6], the authors conduct an error and stability analysis for an operator splitting finite element discretization of (1.2) whilst an error analysis for the semidiscrete Galerkin finite element scheme is presented in [16]. Utilizing a Crank-Nicolson temporal and finite difference spatial discretization of (1.2), a predictor-corrector scheme is studied in [40] and the spherically symmetric case is studied in [25]. In [9], the behaviour of the solution of the Schrödinger-Poisson-Xα system is explored through a discretization based on the time splitting spectral method. A time semidiscrete scheme for (1.2) using Strang splitting is studied extensively in [37] and an error analysis is provided. The Gaussian beams method is introduced in [30] for the numerical simulation of (1.2) in the one dimensional case whilst in [47] error estimates are obtained for a Crank-Nicolson in time, compact finite difference in space discretization of (1.2). A numerical method consisting of a backward Euler in time, pseudo-spectral method in space is utilized in [46] to approximate the ground states and the solution of the Schrödinger-Poisson-Slater system (which also includes (1.2)). A spectral discontinuous Galerkin method in space coupled with a Runge-Kutta scheme in time is used to study solutions of (1.2) in [36].

All of the aforementioned methods for the SPS are implicit with respect to the nonlinear term, which means that a nonlinear system must be solved for their implementation. Also none of the

above methods satisfy a discrete analogue of the energy balance (or the energy conservation) that the continuous problem does. *To the best of our knowledge, at the moment, the literature lacks a numerical method for the Schrödinger-Poisson system that satisfies a discrete analogue of the energy balance of the continuous problem.*

1.3. **Main contribution of this paper.** *In this paper we introduce a novel numerical scheme for the discretization of the SPS* (1.1). In particular, for the spatial discretization we use the standard conforming finite element method, while for the temporal discretization we propose a new Crank-Nicolson relaxation-type method. More precisely, we linearize the nonlinear term $|u|^2 - \mu$ in the potential equation of (1.1) and discretize it using the Crank-Nicolson method. The main advantage of the particular scheme is that it avoids solving a computationally expensive nonlinear system, whilst maintaining the second order temporal accuracy of the Crank-Nicolson method. For the proposition of this method we were inspired by Besse, [10, 11], who used a relaxation-type Crank-Nicolson scheme with constant time-steps for the nonlinear Schrödinger equation. Katsaounis and Kyza in [34] generalised the scheme of [10] to variable time-steps and used it to derive a posteriori error estimates, while Zouraris in [50] used a similar scheme for a semilinear parabolic equation.

In particular, *our main contribution is the proposition of a fully discrete relaxation-type Crank-Nicolson finite element scheme with variable temporal and spatial mesh sizes, which is implicit with respect to the Laplacian terms of* (1.1) *(hence guaranteeing stability), but explicit in the nonlinearity of the potential equation of* (1.1). The fact that the proposed method is with variable temporal and mesh-sizes opens the road for the a posteriori error analysis and the proposition of adaptive algorithms for (1.1); this is the focus of a forthcoming paper. *Our method is easily implementable and is numerically shown to be of second order of accuracy. Moreover, it is proven to inherit on the discrete level the mass conservation and energy balance laws of the original continuous problem, for constant meshes. To the best of our knowledge, this is the first time that such a method, satisfying all the above mentioned properties, is proposed in the literature for the SPS* (1.1). *In fact, to the best of our knowledge this is the first method proposed for the SPS that satisfies a discrete energy law.*

1.4. **Idea behind the scheme.** The scheme is presented in full detail in Section 3, however at this point we can give a heuristic description of the main idea behind it. For example, a semi-discrete fully implicit Crank-Nicolson scheme with constant time-step k for the standard SPS (1.2) could be written as

$$\begin{cases} \dfrac{U^n - U^{n-1}}{k} - \dfrac{i\varepsilon}{2\alpha^2}\Delta U^{n-\frac{1}{2}} + \dfrac{i\beta}{\varepsilon\alpha} V^{n-\frac{1}{2}} U^{n-\frac{1}{2}} = 0, \\ \Delta V^{n-\frac{1}{2}} = |U^{n-\frac{1}{2}}|^2, \end{cases} \tag{1.3}$$

with the usual notation of $U^{n-\frac{1}{2}} := (U^n + U^{n-1})/2$, $V^{n-\frac{1}{2}} := (V^n + V^{n-1})/2$. This might be an interesting scheme (second order in k, mass preserving), but each time-step involves a nonlinear system in the unknowns U^n, v^n and would be computationally expensive and complicated to implement.

So instead of that, the idea here is to use an auxiliary variable on a staggered timegrid. We introduce an auxiliary variable $\Phi^{n-\frac{1}{2}}$ as a proxy for the position density and update it by linear extrapolation

$$\frac{\Phi^{n-\frac{1}{2}} + \Phi^{n-\frac{3}{2}}}{2} = |U^{n-1}|^2, \tag{1.4}$$

then define $V^{n-\frac{1}{2}}$ simply as

$$\Delta V^{n-\frac{1}{2}} = \Phi^{n-\frac{1}{2}}.$$

Thus we end up with a semi-discrete scheme of the form

$$\begin{cases} \Phi^{n-\frac{1}{2}} = 2|U^{n-1}|^2 - \Phi^{n-\frac{3}{2}}, \\ \Delta V^{n-\frac{1}{2}} = \Phi^{n-\frac{1}{2}}, \\ \dfrac{U^n - U^{n-1}}{k} - \dfrac{i\varepsilon}{2\alpha^2}\Delta U^{n-\frac{1}{2}} + \dfrac{i\beta}{\varepsilon\alpha}V^{n-\frac{1}{2}}U^{n-\frac{1}{2}} = 0, \end{cases} \tag{1.5}$$

where the equations above appear in the order they would be solved. For variable time-step, the same idea yields the scheme in (3.2) by adjusting the linear extrapolation step of (1.4).

1.5. **Organization of the paper.** The rest of the paper is organized as follows: In Section 2 we derive the balance laws of the Schrödinger-Poisson system (1.1) while in Section 3 we introduce our new numerical method and derive discrete variants of the system's conservation laws. Section 4 explains the practical implementation of the numerical scheme. In Section 5, we present numerical experiments which verify the accuracy and efficiency of the method. We finish the section by applying the numerical method to a concrete example from cosmology.

2. Mass conservation & Energy balance

The standard Schrödinger-Poisson system (1.2) exhibits mass and energy conservation, consistently with its quantum mechanical interpretation [13]. If however the coefficients $p(t), q(t)$ vary in time, the more general system (1.1) still satisfies mass conservation and exhibits a precise *energy balance law* instead of simple conservation. More specifically, given (1.1) let us define the *mass*

$$\mathcal{M}(t) := \|u(t)\|^2, \tag{2.1}$$

and the *kinetic energy* $\mathcal{E}_k(t)$ and *potential energy* $\mathcal{E}_{\mathsf{v}}(t)$

$$\mathcal{E}_k(t) := \|\nabla u(t)\|^2, \quad \mathcal{E}_{\mathsf{v}}(t) := \|\nabla \mathsf{v}(t)\|^2 \ = -\int_\Omega \mathsf{v}(t)(|u(t)|^2 - \mu)\,\mathrm{d}x, \tag{2.2}$$

where $\|\cdot\|$ denotes the L^2-norm over Ω. It is worth noting that the integration by parts,

$$\int_\Omega \nabla \mathsf{v}(t)\cdot\nabla \mathsf{v}(t)\,\mathrm{d}x = -\int_\Omega \mathsf{v}(t)\Delta \mathsf{v}(t)\,\mathrm{d}x, \tag{2.3}$$

which is used in showing that the two expressions for the potential energy in (2.2) are equivelant, works equally well with both the periodic or the homogeneous Dirichlet boundary conditions. With this at hand, we are now ready to prove the following:

Lemma 2.1 (Continuous Mass Conservation & Energy Balance)**.** *If* (u, v) *is a solution of* (1.1) *then , for* $\tau \le t \le T$

$$\mathcal{M}(t) = \mathcal{M}(\tau), \qquad \textit{Conservation of Mass}, \tag{2.4}$$

$$p(t)\frac{d}{dt}\mathcal{E}_k(t) - \frac{q(t)}{2}\frac{d}{dt}\mathcal{E}_{\mathsf{v}}(t) = 0, \qquad \textit{Balance of Energy}. \tag{2.5}$$

Proof. We begin the proof by deriving conservation of mass. To obtain this, we multiply the Schrödinger equation by $\bar{u}$ and integrate over Ω yielding

$$\int_\Omega \bar{u}u_t\,\mathrm{d}x + \mathrm{i}p(t)\|\nabla u\|^2 + \mathrm{i}q(t)\int_\Omega \mathsf{v}|u|^2\,\mathrm{d}x = 0. \tag{2.6}$$

Since $p(t),\ q(t),\ \mathsf{v}$ are real-valued, taking real parts immediately implies that

$$\int_\Omega (\bar{u}u_t + u\bar{u}_t)\,\mathrm{d}x = 0 \implies \frac{\mathrm{d}}{\mathrm{d}t}\mathcal{M}(t) = 0. \tag{2.7}$$

and (2.4) readily holds.

To derive the energy balance, we begin by differentiating the potential equation with respect to t yielding

$$\Delta \mathsf{v}_t = \frac{\partial}{\partial t}\Big(|u|^2 - \mu\Big) = 2\mathcal{R}e(u\bar{u}_t). \tag{2.8}$$

Multiplying this by v and integrating over Ω we get

$$-\frac{1}{2}\frac{\mathrm{d}}{\mathrm{d}t}\|\nabla \mathsf{v}\|^2 = \int_\Omega \mathsf{v}\Delta \mathsf{v}_t \,\mathrm{d}x = 2\int_\Omega \mathsf{v}\mathcal{R}e(u\bar{u}_t)\,\mathrm{d}x. \tag{2.9}$$

If we now resort to the Schrödinger equation, multiply it by $\bar{u}_t$ and integrate over Ω we obtain

$$\int_\Omega u_t\bar{u}_t \,\mathrm{d}x - \mathrm{i}p(t)\int_\Omega \bar{u}_t\Delta u \,\mathrm{d}x + \mathrm{i}q(t)\int_\Omega \mathsf{v}u\bar{u}_t \,\mathrm{d}x = 0, \tag{2.10}$$

or equivalently,

$$\|u_t\|^2 + \mathrm{i}p(t)\int_\Omega \nabla u\cdot\nabla\bar{u}_t \,\mathrm{d}x + \mathrm{i}q(t)\int_\Omega \mathsf{v}u\bar{u}_t \,\mathrm{d}x = 0. \tag{2.11}$$

Taking imaginary parts yields

$$\frac{1}{2}p(t)\frac{\mathrm{d}}{\mathrm{d}t}\|\nabla u\|^2 + q(t)\int_\Omega \mathsf{v}\mathcal{R}e(u\bar{u}_t)\,\mathrm{d}x = 0. \tag{2.12}$$

We now substitute in (2.9) to get

$$p(t)\frac{\mathrm{d}}{\mathrm{d}t}\|\nabla u\|^2 - \frac{1}{2}q(t)\frac{\mathrm{d}}{\mathrm{d}t}\|\nabla \mathsf{v}\|^2 = 0. \tag{2.13}$$

Using the second expression for the potential energy, namely

$$||\nabla \mathsf{v}||^2 = -\int_\Omega \mathsf{v}\Delta \mathsf{v}\,\mathrm{d}x = -\int_\Omega \mathsf{v}(|u|^2-\mu)\,\mathrm{d}x, \tag{2.14}$$

we can equivalently get

$$p(t)\frac{\mathrm{d}}{\mathrm{d}t}\|\nabla u\|^2 + \frac{1}{2}q(t)\frac{\mathrm{d}}{\mathrm{d}t}\int_\Omega \mathsf{v}(|u|^2-\mu)\,\mathrm{d}x = 0. \tag{2.15}$$

From either (2.13) or (2.15) we obtain the balance of energy (2.5). □

Remark 2.1. *From the previous lemma it's obvious that for p, q constant in time one recovers the energy conservation law*

$$\frac{d}{dt}\left(p\mathcal{E}_k(t) - \frac{q}{2}\mathcal{E}_{\mathsf{v}}(t)\right) = 0 \implies p\mathcal{E}_k(t) - \frac{q}{2}\mathcal{E}_{\mathsf{v}}(t) = p\mathcal{E}_k(\tau) - \frac{q}{2}\mathcal{E}_{\mathsf{v}}(\tau), \quad \tau \le t \le T.$$

3. A new Relaxation-type Numerical Method & Discrete Balance Laws

The numerical scheme we propose here is inspired by the Crank-Nicolson relaxation method introduced by Besse in [10] for the nonlinear Schrödinger equation. The first stage in the creation of a Besse-style relaxation scheme is to rewrite system (1.1) via the introduction of an auxiliary variable $\phi = |u|^2 - \mu$ which takes the place of the nonlinearity. We are thus now searching for a solution (u, v, ϕ) of the following enlarged Schrödinger-Poisson system

$$\begin{cases} u_t - \mathrm{i}p(t)\Delta u + \mathrm{i}q(t)\mathsf{v}u = 0, & \text{in } \Omega\times(\tau,T),\\ \Delta \mathsf{v} = \phi, & \text{in } \Omega\times(\tau,T),\\ \phi = |u|^2 - \mu, & \text{in } \Omega\times(\tau,T),\\ u(\mathbf{x},\tau) = u_0(\mathbf{x}), & \text{in } \Omega,\\ \{\mu = 0 \text{ and } u = \mathsf{v} = 0\}, \ \text{ OR } \ \{\mu = \|u_0\|_{L^2}^2 \text{ and } u, \mathsf{v} \text{ periodic, }\} & \text{on } \partial\Omega\times(\tau,T], \end{cases} \tag{3.1}$$

which is, obviously, equivalent to the original problem (1.1). The numerical scheme that we will introduce in the sequel is based upon this enlarged formulation of the Schrödinger-Poisson system. For the remainder of this section, we assume (1.1)/(3.1) to be augmented with zero Dirichlet boundary conditions for the simplicity of the presentation only as the modification of the numerical method to incorporate periodic boundary conditions is standard. We begin by first presenting the time semi-discrete scheme before moving on to the presentation of the fully-discrete scheme.

3.1. **Time semi-discrete scheme.** We introduce a sequence of $N+1$ *time nodes* $\tau =: t_0 < ... < t_n < \ldots < t_N := T$ of $[\tau, T]$ and the variable time-steps $k_n := t_n - t_{n-1}$. With this notation, our time semi-discrete Besse-style relaxation scheme for (1.1) based on (3.1) is defined as follows: We seek approximations $(U^n, V^{n-1/2}, \Phi^{n-1/2}) \in H_0^1(\Omega)$ to $(u(t_n), \mathsf{v}(t_{n-1/2}), \phi(t_{n-1/2})) \in H_0^1(\Omega)$, $1 \le n \le N$, such that

$$
\begin{cases}
\overline{\partial} U^n - \mathrm{i} p(t_{n-1/2}) \Delta U^{n-1/2} + \mathrm{i} q(t_{n-1/2}) V^{n-1/2} U^{n-1/2} = 0, \\
\Delta V^{n-1/2} = \Phi^{n-1/2}, \\
\dfrac{k_{n-1}}{k_{n-1}+k_n} \Phi^{n-1/2} = (|U^{n-1}|^2 - \mu) - \dfrac{k_n}{k_{n-1}+k_n} \Phi^{n-3/2},
\end{cases}
\tag{3.2}
$$

holds, where we used the notation

$$
t_{n-1/2} := \frac{t_{n-1}+t_n}{2}, \quad U^{n-1/2} := \frac{U^{n-1}+U^n}{2}, \quad \overline{\partial} U^n := \frac{U^n - U^{n-1}}{k_n}.
\tag{3.3}
$$

The scheme should be initialized at $n = 0$; a natural, straightforward choice is $U^0 = u_0$, $k_0 = k_1$, $\Phi^{-1/2} = |u_0|^2 - \mu$. In Section 4.1 we discuss some subtle computational issues with this initialization, and derive a modified initialization which addresses them.

Remark 3.1. Method (3.2) can be combined with various methods for spatial discretization. Examples include finite differences, in the spirit of [10, 50], spectral methods, or finite elements. In this paper we choose finite elements for the spatial discretization, which allow for spatial adaptivity; this is particularly important for the Schrödinger-Poisson system (1.1) with applications in cosmology, in which we observe sharply localized features for the density (cf. Section 5.4).

3.2. **Fully-discrete scheme.** Let $\mathcal{T}_h$ be a conforming, shape regular partition of Ω consisting of elements K which are either simplices or d-dimensional cubes. We then build real/complex finite element spaces over the mesh $\mathcal{T}_h$, denoted by $\mathcal{V}_h(\mathcal{T}_h; \mathbb{R})$ and $\mathcal{V}_h(\mathcal{T}_h; \mathbb{C})$, respectively, given by

$$
\begin{aligned}
\mathcal{V}_h(\mathcal{T}_h; \mathbb{R}) &:= \big\{ \chi \in C(\bar{\Omega}) \cap H_0^1(\Omega) : \forall K \in \mathcal{T}_h,\ \chi|_K \in \mathbb{P}^r(K) \big\}, \\
\mathcal{V}_h(\mathcal{T}_h; \mathbb{C}) &:= \{ \chi_R + \mathrm{i}\chi_I : \chi_R, \chi_I \in \mathcal{V}_h(\mathcal{T}_h; \mathbb{R}) \},
\end{aligned}
\tag{3.4}
$$

where $\mathbb{P}^r(K)$ denotes the space of polynomials on the element K of total degree r if K is a simplex or of degree r in each variable if K is a d-dimensional cube. At each time step n, we assume that we have some mesh $\mathcal{T}_h^n$ which has been obtained from a previous mesh $\mathcal{T}_h^{n-1}$ via a limited number of refinement and/or coarsening operations. We then associate to each time step n the real and complex finite element spaces $\mathcal{V}_h^n(\mathbb{R}) := \mathcal{V}_h(\mathcal{T}_h^n; \mathbb{R})$ and $\mathcal{V}_h^n(\mathbb{C}) := \mathcal{V}_h(\mathcal{T}_h^n; \mathbb{C})$ over the mesh $\mathcal{T}_h^n$.

To characterize the fully-discrete scheme on (possibly) variable finite element spaces, we need to introduce two operators; namely, the L^2-projection operator $\mathcal{P}_h^n : L^2(\Omega) \to \mathcal{V}_h^n(\mathbb{C})$ and the discrete Laplacian operator $-\Delta_h^n : H_0^1(\Omega) \to \mathcal{V}_h^n(\mathbb{C})$, which are defined implicitly as the solution of the following variational problems

$$
v \mapsto \mathcal{P}_h^n v, \qquad \langle \mathcal{P}_h^n v, \chi^n \rangle = \langle v, \chi^n \rangle, \qquad \forall \chi^n \in \mathcal{V}_h^n(\mathbb{R}),
\tag{3.5}
$$

$$
v \mapsto -\Delta_h^n v, \qquad \langle -\Delta_h^n v, \chi^n \rangle = \langle \nabla v, \nabla \chi^n \rangle, \qquad \forall \chi^n \in \mathcal{V}_h^n(\mathbb{R}),
\tag{3.6}
$$

where $\langle \cdot, \cdot \rangle$ denotes the L^2-inner product over Ω. Note that although the L^2-projection/discrete Laplacian may be complex in the above definitions, the test functions always lie in the real finite element space $\mathcal{V}_h^n(\mathbb{R})$. We are now ready to introduce the fully-discrete Besse-style relaxation scheme for (1.2) based on (3.1) which is given as follows: We seek approximations $(U_h^n, V_h^{n-1/2}, \Phi_h^{n-1/2}) \in \mathcal{V}_h^n(\mathbb{C}) \times \mathcal{V}_h^n(\mathbb{R}) \times \mathcal{V}_h^n(\mathbb{R})$ to $(u(\cdot, t_n), \mathsf{v}(\cdot, t_{n-1/2}), \phi(\cdot, t_{n-1/2})) \in H_0^1(\Omega)$, $1 \le n \le N$, such that

$$
\begin{cases}
\mathcal{P}_h^n \left[\overline{\partial} U_h^n - \dfrac{\mathrm{i}}{2} p(t_{n-1/2}) (\Delta_h^{n-1} U_h^{n-1} + \Delta_h^n U_h^n) + \mathrm{i} q(t_{n-1/2}) V_h^{n-1/2} U_h^{n-1/2} \right] = 0, \\
\Delta_h^n V_h^{n-1/2} = \Phi_h^{n-1/2}, \\
\dfrac{k_{n-1}}{k_{n-1}+k_n} \Phi_h^{n-1/2} = \mathcal{P}_h^n \left[(|U_h^{n-1}|^2 - \mu) - \dfrac{k_n}{k_{n-1}+k_n} \Phi_h^{n-3/2} \right],
\end{cases}
\tag{3.7}
$$

where the straightforward initialization would be $U_h^0 = \mathcal{P}_h^0 u_0$, $k_0 = k_1$ and $\Phi_h^{-1/2} = \mathcal{P}_h^0(|u_0|^2 - \mu)$. If no mesh change occurs on the time step n, i.e., $\mathcal{T}_h^n = \mathcal{T}_h^{n-1}$ then the fully-discrete Besse-style relaxation scheme (3.7) can be simplified to

$$\begin{cases} \overline{\partial} U_h^n - \mathrm{i}p(t_{n-1/2})\Delta_h^n U_h^{n-1/2} + \mathrm{i}q(t_{n-1/2})\mathcal{P}_h^n(V_h^{n-1/2}U_h^{n-1/2}) = 0, \\ \Delta_h^n V_h^{n-1/2} = \Phi_h^{n-1/2}, \\ \dfrac{k_{n-1}}{k_{n-1}+k_n}\Phi_h^{n-1/2} = \mathcal{P}_h^n(|U_h^{n-1}|^2 - \mu) - \dfrac{k_n}{k_{n-1}+k_n}\Phi_h^{n-3/2}. \end{cases} \tag{3.8}$$

We now look into whether the numerical scheme (3.8) satisfies discrete versions of the system's conservation laws (cf. Lemma 2.1 for the continuous version).

The *discrete mass* is the discrete equivalent of the mass (2.1) and is given by

$$\mathcal{M}_h^n := ||U_h^n||^2. \tag{3.9}$$

The discrete mass satisfies an exact equivalent of the conservation of mass law, as is seen in the following:

Proposition 3.1 (Discrete Mass Conservation)**.** *If no mesh change occurs on the time step n, i.e. if $\mathcal{T}_h^n = \mathcal{T}_h^{n-1}$, then the solution of the fully-discrete Besse-style relaxation scheme* (3.8) *satisfies*

$$\mathcal{M}_h^n = \mathcal{M}_h^{n-1}.$$

Therefore, if no mesh change occurs at all, i.e. if $\mathcal{T}_h^n = \mathcal{T}_h^0$, $\forall 1 \le n \le N$, then

$$\mathcal{M}_h^n = \mathcal{M}_h^0, \quad 1 \le n \le N. \tag{3.10}$$

Proof. We multiply the discrete Schrödinger equation in (3.8) by $\overline{U}_h^{n-1/2}$, i.e, the complex conjugate of $U_h^{n-1/2}$ and integrate over Ω to obtain

$$\int_\Omega \overline{U}_h^{n-1/2}\overline{\partial} U_h^n \,\mathrm{d}x + \mathrm{i}p(t_{n-1/2})||\nabla U_h^{n-1/2}||^2 + \mathrm{i}q(t_{n-1/2})\int_\Omega V_h^{n-1/2}|U_h^{n-1/2}|^2 \,\mathrm{d}x = 0. \tag{3.11}$$

The last two terms are purely imaginary so taking real parts and expanding yields

$$\mathcal{M}_h^n - \mathcal{M}_h^{n-1} + \int_\Omega \mathcal{R}e(U_h^n\overline{U}_h^{n-1} - U_h^{n-1}\overline{U}_h^n)\,\mathrm{d}x = 0. \tag{3.12}$$

The last integral vanishes and so we are left with

$$\mathcal{M}_h^n = \mathcal{M}_h^{n-1}, \tag{3.13}$$

as claimed. □

The *discrete energy balance* is slightly more sophisticated, as more can be said about how to discretize the energy. In equation (2.2), two expressions for the potential energy were given; both of them come into play, but at the discrete level they are not necessarily identical. In that context, we will define the *discrete kinetic energy* $\mathcal{E}_{k,h}^n$, and the two *discrete versions of the potential energy* $\mathcal{E}_{\mathsf{v}_1,h}^n, \mathcal{E}_{\mathsf{v}_2,h}^n$ as follows:

$$\mathcal{E}_{k,h}^n = \|\nabla U_h^n\|^2, \quad \mathcal{E}_{\mathsf{v}_1,h}^n = \|\nabla V_h^{n-1/2}\|^2 \quad \mathcal{E}_{\mathsf{v}_2,h}^n = -\int_\Omega V_h^{n-1/2}(|U_h^n|^2 - \mu)\,\mathrm{d}x. \tag{3.14}$$

What will end up playing the role of *the discrete potential energy* would be $\mathcal{E}_{\mathsf{v},h}^n := 2\mathcal{E}_{\mathsf{v}_2,h}^n - \mathcal{E}_{\mathsf{v}_1,h}^n$. We are now ready to prove the following

Proposition 3.2 (Discrete Energy Balance)**.** *Assume that the time-step size remains constant between successive time-steps, i.e $k_{n-1} = k_n$, and that no mesh change occurs on time step n, i.e. $\mathcal{T}_h^n = \mathcal{T}_h^{n-1}$. Then the solution of the fully-discrete relaxation scheme* (3.8) *satisfies the discrete energy balance law*

$$p(t_{n-1/2})\overline{\partial}(\mathcal{E}_{k,h}^n) - \frac{q(t_{n-1/2})}{2}\overline{\partial}\left(2\mathcal{E}_{\mathsf{v}_2,h}^n - \mathcal{E}_{\mathsf{v}_1,h}^n\right) = 0, \tag{3.15}$$

which is the discrete analog of (2.5)*.*

If furthermore p, q are constants, (3.15) *simplifies to*

$$p\mathcal{E}^n_{k,h}-\frac{q}{2}(2\mathcal{E}^n_{\mathsf{v}_2,h}-\mathcal{E}^n_{\mathsf{v}_1,h})=p\mathcal{E}^{n-1}_{k,h}-\frac{q}{2}(2\mathcal{E}^{n-1}_{\mathsf{v}_2,h}-\mathcal{E}^{n-1}_{\mathsf{v}_1,h}). \tag{3.16}$$

Finally, if in addition the time-step size and spatial mesh do not change over the whole computation, i.e. if $k_n = k$ and $\mathcal{T}^n_h = \mathcal{T}_h$ for all $n = 1, 2, \dots, N$, then

$$p\mathcal{E}^n_{k,h}+\frac{q}{2}(2\mathcal{E}^n_{\mathsf{v}_2,h}-\mathcal{E}^n_{\mathsf{v}_1,h})=p\mathcal{E}^1_{k,h}+\frac{q}{2}(2\mathcal{E}^1_{\mathsf{v}_2,h}-\mathcal{E}^1_{\mathsf{v}_1,h}). \tag{3.17}$$

Proof. Multiplying the discrete Schrödinger equation (3.8) by $\overline{\partial}\,\overline{U}^n_h$ and integrating over Ω we obtain

$$\|\overline{\partial}U^n_h\|^2+\mathrm{i}p(t_{n-1/2})\int_\Omega \nabla U^{n-1/2}_h\cdot\nabla\overline{\partial}\,\overline{U}^n_h\,\mathrm{d}x+\mathrm{i}q(t_{n-1/2})\int_\Omega V^{n-1/2}_h U^{n-1/2}_h\overline{\partial}\,\overline{U}^n_h\,\mathrm{d}x=0.$$

Taking imaginary parts yields

$$\frac{p(t_{n-1/2})}{2k_n}(\|\nabla U^n_h\|^2-\|\nabla U^{n-1}_h\|^2)+\frac{q(t_{n-1/2})}{2k_n}\int_\Omega V^{n-1/2}_h(|U^n_h|^2-|U^{n-1}_h|^2)\,\mathrm{d}x=0. \tag{3.18}$$

For the second term of (3.18) we have

$$\begin{aligned}
&\int_\Omega V^{n-1/2}_h(|U^n_h|^2-|U^{n-1}_h|^2)\,\mathrm{d}x=\int_\Omega V^{n-1/2}_h\left((|U^n_h|^2-\mu)-(|U^{n-1}_h|^2-\mu)\right)\,\mathrm{d}x\\
&=\int_\Omega\left(V^{n-1/2}_h(|U^n_h|^2-\mu)-V^{n-3/2}_h(|U^{n-1}_h|^2-\mu)\right)\,\mathrm{d}x\\
&+\int_\Omega\left(V^{n-3/2}_h(|U^{n-1}_h|^2-\mu)-V^{n-1/2}_h(|U^{n-1}_h|^2-\mu)\right)\,\mathrm{d}x\\
&=\int_\Omega k_n\,\overline{\partial}\left(V^{n-1/2}_h(|U^n_h|^2-\mu)\right)\,\mathrm{d}x+\int_\Omega(|U^{n-1}_h|^2-\mu)(V^{n-3/2}_h-V^{n-1/2}_h)\,\mathrm{d}x
\end{aligned}$$

Hence (3.18) becomes

$$\begin{aligned}
&\frac{p(t_{n-1/2})}{2}\overline{\partial}(\|\nabla U^n_h\|^2)+\\
&\quad+\frac{q(t_{n-1/2})}{2k_n}\left(\int_\Omega k_n\overline{\partial}\left(V^{n-1/2}_h(|U^n_h|^2-\mu)\right)\,\mathrm{d}x+\int_\Omega(|U^{n-1}_h|^2-\mu)(V^{n-3/2}_h-V^{n-1/2}_h)\,\mathrm{d}x\right)=0.
\end{aligned} \tag{3.19}$$

Using (3.7)(c), (3.7)(b), and finally integration by parts, for the third term of (3.19) we obtain,

$$\begin{aligned}
&\int_\Omega(|U^{n-1}_h|^2-\mu)(V^{n-3/2}_h-V^{n-1/2}_h)\,\mathrm{d}x=\int_\Omega\mathcal{P}^n_h\left(|U^{n-1}_h|^2-\mu\right)(V^{n-3/2}_h-V^{n-1/2}_h)\,\mathrm{d}x\\
&=\int_\Omega\left(\frac{k_{n-1}}{k_{n-1}+k_n}\Phi^{n-1/2}_h+\frac{k_n}{k_{n-1}+k_n}\Phi^{n-3/2}_h\right)(V^{n-3/2}_h-V^{n-1/2}_h)\,\mathrm{d}x\\
&=\int_\Omega\left(\frac{k_{n-1}}{k_{n-1}+k_n}\Delta^n_hV^{n-1/2}_h+\frac{k_n}{k_{n-1}+k_n}\Delta^n_hV^{n-3/2}_h\right)(V^{n-3/2}_h-V^{n-1/2}_h)\,\mathrm{d}x\\
&=\int_\Omega\left(\frac{k_{n-1}}{k_{n-1}+k_n}\nabla V^{n-1/2}_h+\frac{k_n}{k_{n-1}+k_n}\nabla V^{n-3/2}_h\right)(\nabla V^{n-1/2}_h-\nabla V^{n-3/2}_h)\,\mathrm{d}x.
\end{aligned} \tag{3.20}$$

Since the time-step size is constant between successive time-steps we readily obtain that

$$\int_\Omega(|U^{n-1}_h|^2-\mu)(V^{n-3/2}_h-V^{n-1/2}_h)\,\mathrm{d}x=\frac{1}{2}\int_\Omega\left(|\nabla V^{n-1/2}_h|^2-|\nabla V^{n-3/2}_h|^2\right)\,\mathrm{d}x=\frac{1}{2}k_n\overline{\partial}(\|\nabla V^{n-1/2}_h\|^2)$$

Using the above to reformulate the last term of (3.19) yields

$$\frac{p(t_{n-1/2})}{2}\overline{\partial}(\|\nabla U^n_h\|^2)+\frac{q(t_{n-1/2})}{2k_n}\left(k_n\int_\Omega\overline{\partial}\left(V^{n-1/2}_h(|U^n_h|^2-\mu)\right)\,\mathrm{d}x+\frac{k_n}{2}\overline{\partial}(\|\nabla V^{n-1/2}_h\|^2)\right)=0.$$

The result then follows from the definition of the discrete energies $\mathcal{E}^n_{k,h}$, $\mathcal{E}^n_{\mathsf{v}_1,h}$, $\mathcal{E}^n_{\mathsf{v}_2,h}$, (3.14). □

Remark 3.2 (Discrete balance laws & periodic boundary conditions)**.** Propositions 3.1 & 3.2 remain valid for the fully discrete scheme corresponding to (1.1)/(3.1) with periodic boundary conditions, as long as the finite element space $\mathcal{V}_h(\mathcal{T}_h;\mathbb{C})$ is appropriately equipped with periodic boundary conditions instead of homogeneous Dirichlet.

An important question that raises here is what happens to the discrete energy balance in the case of variable time-steps. In particular, by how much does it fail to satisfy (3.15)? We answer this in the next proposition:

Proposition 3.3 (Discrete Energy Balance & Variable time-steps)**.** *Assume that no mesh change occurs on time step n, i.e. $\mathcal{T}_h^n = \mathcal{T}_h^{n-1}$. Then the solution of the fully-discrete relaxation scheme* (3.8) *satisfies the following*

$$p(t_{n-1/2})\overline{\partial}(\mathcal{E}_{k,h}^n) - \frac{q(t_{n-1/2})}{2}\overline{\partial}\left(2\mathcal{E}_{\mathsf{v}_2,h}^n - \mathcal{E}_{\mathsf{v}_1,h}^n\right) + \frac{q(t_{n-1/2})}{4}\frac{k_{n-1}-k_n}{k_{n-1}+k_n}k_n\|\bar{\partial}\nabla V_h^{n-1/2}\|^2 = 0. \tag{3.21}$$

Proof. For this case, (3.19) and (3.20) are still valid. From (3.20) we obtain

$$\begin{aligned}
&\int_\Omega (|U_h^{n-1}|^2-\mu)(V_h^{n-3/2}-V_h^{n-1/2})\,\mathrm{d}x = \int_\Omega \mathcal{P}_h^n\Big(|U_h^{n-1}|^2-\mu\Big)(V_h^{n-3/2}-V_h^{n-1/2})\,\mathrm{d}x\\
=&\int_\Omega\left(\frac{k_{n-1}}{k_{n-1}+k_n}\Phi_h^{n-1/2}+\frac{k_n}{k_{n-1}+k_n}\Phi_h^{n-3/2}\right)(V_h^{n-3/2}-V_h^{n-1/2})\,\mathrm{d}x\\
=&\frac{1}{2}k_n\overline{\partial}(\|\nabla V_h^{n-1/2}\|^2)+\frac{k_{n-1}-k_n}{2(k_{n-1}+k_n)}\int_\Omega(\nabla V_h^{n-1/2}-\nabla V_h^{n-3/2})^2\,\mathrm{d}x\\
=&\frac{1}{2}k_n\overline{\partial}(\|\nabla V_h^{n-1/2}\|^2)+\frac{k_{n-1}-k_n}{2(k_{n-1}+k_n)}k_n^2\|\bar{\partial}\nabla V_h^{n-1/2}\|^2.
\end{aligned}$$

Using the above to reformulate the last term of (3.19) we obtain (3.21). □

Remark 3.3. Clearly, if $k_{n-1}=k_n$ (3.21) reduces to (3.15). For variable time-steps the remainder term $\frac{q(t_{n-1/2})}{4}\frac{k_{n-1}-k_n}{k_{n-1}+k_n}k_n\|\bar{\partial}\nabla V_h^{n-1/2}\|^2$ is expected to be of first order in time; in other words, the energy balance law (3.15) fails to be satisfied by order $\mathcal{O}(k)$ (where $k=\max_{1\le n\le N-1}k_n$), every time we change the time-step.

4. Implementation

In this section, we discuss the practicalities of implementing the Besse-style relaxation scheme (3.7) for the numerical solution of the Schrödinger-Poisson system (1.2).

4.1. **Initialization.** In Section 3, the straightforward initialization $U_h^0=\mathcal{P}_h^0u_0$, $k_0=k_1$ and $\Phi_h^{-1/2}=\mathcal{P}_h^0(|u_0|^2-\mu)$ was presented. This is a simple, viable choice, and we observe numerically that the obtained numerical solution U^n is a second order approximation in time to $u(t_n)$. However, in the same computations we observe that $\Phi^{n-\frac{1}{2}}$ is only a first order approximation in time to $\mathsf{v}(t_{n-1/2})$. This is something also observed in [50]. Thus we look for a modified initialization under which both U^n and $\Phi^{n-\frac{1}{2}}$ will be seen numerically to be of second order in time.

One way to do this is to define $\Phi_{h,\mathrm{old}}^{1/2}$ according to the straightforward initialization, i.e. $\Phi_{h,\mathrm{old}}^{1/2}=\mathcal{P}_h^0(|u_0|^2-\mu)$. $\Phi_{h,\mathrm{old}}^{1/2}$ is then used in the numerical scheme (3.7) to calculate initial approximations for the potential and wavefunction which we denote by $\widetilde{V}_h^{1/2}$ and $\widetilde{U}_h^1$, respectively. The initial approximation to the wavefunction, $\widetilde{U}_h^1$, is then used to update the estimate for the nonlinearity on the first time step. In particular, the coefficients $\widehat{\Phi}_h^{1/2}$ are chosen to satisfy

$$M\widehat{\Phi}_h^{1/2} = \left(\left\langle\frac{1}{2}(|\widetilde{U}_h^1|^2-\mu)+\frac{1}{2}\Phi_{h,\mathrm{old}}^{1/2},\varphi_j^1\right\rangle_{j=1,\dots,\mathcal{N}_1}\right). \tag{4.1}$$

This is equivalent to choosing a modified

$$\Phi_h^{-1/2} = \frac{3}{2}\left(|U_h^0|^2-\mu\right)-\frac{1}{2}\left(|\widetilde{U}_h^1|^2-\mu\right) \tag{4.2}$$

to be used in (3.7)(c). Using this initialization we observe numerically second order in time for both U^n, $\Phi^{n-\frac{1}{2}}$. An analogous initialization can be found in [50] for a Besse-type relaxation finite difference scheme and the semilinear parabolic equation.

4.2. **Solving for the nonlinearity.** Solving for the nonlinearity is a standard finite element problem, i.e., we are seeking a vector of coefficients $\widehat{\Phi}_h^{n-1/2}$ for $\Phi_h^{n-1/2}$ such that

$$\Phi_h^{n-1/2} = \sum_{j=1}^{\mathcal{N}_n} \widehat{\Phi}_{h,j}^{n-1/2} \varphi_j^n,$$

where φ_j^n, $j = 1, \dots, \mathcal{N}_n = \dim(\mathcal{V}_h^n(\mathbb{R}))$ are (real) finite element basis functions. From (3.7), we see that the vector of coefficients $\widehat{\Phi}_h^{n-1/2}$ must satisfy

$$\frac{k_{n-1}}{k_{n-1}+k_n} M \widehat{\Phi}_h^{n-1/2} = \left(\left\langle |U_h^{n-1}|^2 - \frac{k_n}{k_{n-1}+k_n} \Phi_h^{n-3/2}, \varphi_j^n \right\rangle_{j=1,\dots,\mathcal{N}_n} \right),$$

where M is the *mass matrix* given by

$$M_{ij} = \int_\Omega \varphi_i^n \varphi_j^n \, \mathrm{d}x.$$

4.3. **Solving for the potential.** Solving for the potential is also fairly routine; if we introduce the vector of coefficients $\widehat{V}_h^{n-1/2}$ such that

$$V_h^{n-1/2} = \sum_{j=1}^{\mathcal{N}_n} \widehat{V}_{h,j}^{n-1/2} \varphi_j^n,$$

then (3.7) implies that $\widehat{V}_h^{n-1/2}$ must satisfy

$$L \widehat{V}_h^{n-1/2} = \left(\langle \Phi_h^{n-1/2}, \varphi_j^n \rangle_{j=1,\dots,\mathcal{N}_n} \right),$$

where L is the *stiffness matrix* given by

$$L_{ij} = \int_\Omega \nabla \varphi_i^n \cdot \nabla \varphi_j^n \, \mathrm{d}x.$$

For V_h^0, the coefficients $\widehat{V}_h^0$ are chosen to satisfy the matrix-vector system

$$L \widehat{V}_h^0 = \left(\langle \Phi_{h,\mathrm{old}}^{1/2}, \varphi_j^0 \rangle_{j=1,\dots,\mathcal{N}_0} \right). \tag{4.3}$$

Another question now is how to use the nodal values $V_h^{n-1/2}$ in order to obtain optimal (second) order approximations V_h^n to $\mathsf{v}(t_n)$ (note that that the obtained by the method approximations $V_h^{n-1/2}$ are approximations to $\mathsf{v}(t_{n-1/2})$, i.e., are approximations at the middle nodal points $t_{n-1/2}$ and not at the nodes t_n). To obtain V_h^1, the most obvious choice is to linearly extrapolate from V_h^0 and $V_h^{1/2}$ to obtain V_h^1, i.e., we set $V_h^1 = 2V_h^{1/2} - V_h^0$. It is tempting to continue to iterate this procedure in order to compute the remaining nodal values, however, for $n \neq 0$, the value V_h^n is an *extrapolated quantity* (in contrast to V_h^0 which is computed according to (4.3)). Attempting to calculate V_h^n by extrapolating through V_h^{n-1} (an extrapolated point) and $V_h^{n-1/2}$ (a computed point) is therefore an unstable procedure which oscillates out of control. To avoid this, we instead calculate V_h^n by linearly extrapolating from the computed values $V_h^{n-1/2}$ and $V_h^{n-3/2}$; a simple calculation yields

$$V_h^n = V_h^{n-1/2} + \frac{k_n}{k_{n-1}+k_n}(V_h^{n-1/2} - V_h^{n-3/2}).$$

4.4. **Solving for the wavefunction.** In the case of the wavefunction, we are seeking a vector of real coefficients $\widehat{U}^n_{h,R}$ and a vector of imaginary coefficients $\widehat{U}^n_{h,I}$ such that

$$U^n_h = U^n_{h,R} + iU^n_{h,I} = \sum_{j=1}^{\mathcal{N}_n} \big(\widehat{U}^n_{h,R,j} + i\widehat{U}^n_{h,I,j}\big)\varphi^n_j.$$

Here, as before, φ^n_j, $j = 1, \ldots, \mathcal{N}_n = \dim(\mathcal{V}^n_h(\mathbb{R}))$ are *real* finite element basis functions which form a basis for $\mathcal{V}^n_h(\mathbb{R})$. Then (3.7) implies that the coefficient vectors must satisfy the block matrix-vector system

$$\begin{aligned}
&\begin{pmatrix} M & \frac{p(t_{n-1/2})k_n}{2}L - \frac{q(t_{n-1/2})k_n}{2}P \\ -\frac{p(t_{n-1/2})k_n}{2}L + \frac{q(t_{n-1/2})k_n}{2}P & M \end{pmatrix}\begin{pmatrix} \widehat{U}^n_{h,R} \\ \widehat{U}^n_{h,I} \end{pmatrix} = \\
&\begin{pmatrix} \big\langle U^{n-1}_{h,R} - \frac{p(t_{n-1/2})k_n}{2}\Delta^{n-1}_h U^{n-1}_{h,I} - \frac{q(t_{n-1/2})k_n}{2}V^{n-1/2}_h U^{n-1}_{h,I}, \varphi^n_j \big\rangle_{j=1,\ldots,\mathcal{N}_n} \\ \big\langle U^{n-1}_{h,I} + \frac{p(t_{n-1/2})k_n}{2}\Delta^{n-1}_h U^{n-1}_{h,R} + \frac{q(t_{n-1/2})k_n}{2}V^{n-1/2}_h U^{n-1}_{h,R}, \varphi^n_j \big\rangle_{j=1,\ldots,\mathcal{N}_n} \end{pmatrix},
\end{aligned} \tag{4.4}$$

where Δ^{n-1}_h is the discrete Laplacian operator (see (3.6)), L is the stiffness matrix and P, the matrix associated with the potential term, is given by

$$P_{ij} = \int_\Omega V^{n-1/2}_h \varphi^n_i \varphi^n_j \, \mathrm{d}x.$$

As is standard, one can extend the nodal values of the wavefunction to a function $U_h(t)$ on the whole interval via linear interpolation, viz.,

$$U_h(t) := \left(\frac{t_n - t}{k_n}\right)U^{n-1}_h + \left(\frac{t - t_{n-1}}{k_n}\right)U^n_h, \qquad t \in [t_{n-1}, t_n].$$

As a side, we note that (4.4) can be solved far more efficiently if no mesh change has occurred Indeed, in this case the system (3.7) can be rewritten to solve for the half point $U^{n-1/2}_h$ (3.8) resulting in the block matrix-vector system

$$\begin{pmatrix} M & -\frac{p(t_{n-1/2})k_n}{2}L - \frac{q(t_{n-1/2})k_n}{2}P \\ \frac{p(t_{n-1/2})k_n}{2}L + \frac{q(t_{n-1/2})k_n}{2}P & M \end{pmatrix}\begin{pmatrix} \widehat{U}^{n-1/2}_{h,R} \\ \widehat{U}^{n-1/2}_{h,I} \end{pmatrix} = \begin{pmatrix} M & 0 \\ 0 & M \end{pmatrix}\begin{pmatrix} \widehat{U}^{n-1}_{h,R} \\ \widehat{U}^{n-1}_{h,I} \end{pmatrix}.$$

The nodal value coefficients $\widehat{U}^n_h$ can then be recovered via $\widehat{U}^n_h = 2\widehat{U}^{n-1/2}_h - \widehat{U}^{n-1}_h$.

5. Numerical Experiments

We perform four sets of numerical experiments. First of all we apply the new numerical method (3.7) to some relatively simple problems in order to confirm numerically the rate of convergence. In addition, we verify the validity of the discrete conservation laws, for both time-independent and time-dependent coefficients p and q. It must be noted that in what follows we use the modified initialization discussed in Section 4.1. We also study how variable time-step affects the conservation of mass and balance of energy.

Moreover, we apply (3.7) to an example with time-dependent coefficients, periodic boundary conditions and singular features ("sine wave collapse") which arises in cosmology. In that context, the semiclassical Schrödinger-Poisson system (1.2) is used as a lower dimensional analogue of the Vlasov-Poisson system [35]. The numerical results reported in this section take place in two spatial dimensions and utilize a C++ code based on the `deal.II` finite element library [8].

5.1. **Experimental order of convergence.** To verify the experimental order of convergence of the numerical method, we apply the classical method of manufactured solutions, i.e., we choose a wavefunction $u(\mathbf{x}, t) : \Omega \times [0, T] \to \mathbb{C}$ and a potential $\mathtt{v}(\mathbf{x}, t) : \Omega \times [0, T] \to \mathbb{R}$ such that (1.2) is satisfied (with the inclusion of appropriate right-hand sides). Note that in this case $\mu = 0$ and homogeneous Dirichlet boundary conditions are used. Moreover we set $\Omega = (-1, 1)^2 \subset \mathbb{R}^2$ and consider uniform partitions $\mathcal{T}_h$ of Ω consisting of squares with sides of length h. For simplicity, we set the PDE coefficients to $\alpha = \beta = \varepsilon = 1$; this leads to $p(t) = \frac{1}{2}$, $q(t) = 1, \forall t$. The initial time is

set to be $\tau = 0$ and the final time is given by $T = 1$. The time interval (τ, T) is subdivided into uniform intervals of time step length $k = T/N > 0$. Then, we choose the right-hand sides such that the exact solution to (1.2) is given by

$$\mathsf{v}(x, y, t) = e^{-t} \sin(\pi(x^2 - 1)(y^2 - 1)), \qquad u(x, y, t) = (1 + i)\mathsf{v}(x, y, t). \tag{5.1}$$

The errors are then measured in the $L^\infty(L^2)$ norm and we expect that

$$e(u; h, k) := \max_{0\le n\le N} \|u(\cdot, t_n) - U_h^n\| = \mathcal{O}(k^2 + h^{r+1}), \quad e(\mathsf{v}; h, k) := \max_{0\le n\le N} \|\mathsf{v}(\cdot, t_n) - V_h^n\| = \mathcal{O}(k^2 + h^{r+1}),$$

where r is the polynomial degree of the spatial finite element space $\mathcal{V}_h(\mathcal{T}_h; \mathbb{R})$.

To compute the spatial convergence rate, we take a large number of time steps, $N = 2000$ i.e. $k = 5 \cdot 10^{-4}$, so that the temporal part of the error is negligible. We then compute the spatial experimental order of convergence by performing two different realizations with the mesh sizes h_1 and h_2 and computing

$$\text{Rate} := \frac{\log(e(\cdot\,; h_1, k)) - \log(e(\cdot\,; h_2, k))}{\log(h_1) - \log(h_2)}.$$

In Table 1, the spatial experimental orders of convergence are displayed for $r = 1$ and $r = 2$. The optimal rate of convergence is observed in both cases (two for $r = 1$ and three for $r = 2$) thus validating the claimed spatial accuracy of our new numerical method (3.7).

TABLE 1. Spatial experimental orders of convergence for u, v.

	$r = 1$				$r = 2$			
h	$e(u; k, h)$	Rate	$e(\mathsf{v}; k, h)$	Rate	$e(u; k, h)$	Rate	$e(\mathsf{v}; k, h)$	Rate
0.250000	2.60203e-1	-	1.36736e-1	-	1.54310e-2	-	8.50485e-3	-
0.125000	6.58945e-2	1.981	3.29791e-2	2.052	2.19359e-3	2.814	1.31987e-3	2.688
0.062500	1.68103e-2	1.971	8.23356e-3	2.002	2.54266e-4	3.109	1.71600e-4	2.943
0.031250	4.22146e-3	1.994	2.05895e-3	2.000	3.12572e-5	3.024	2.16460e-5	2.987
0.015625	1.05487e-3	2.001	5.14783e-4	2.000	3.85637e-6	3.019	2.71179e-6	2.997

For the temporal error rate, we take a large polynomial degree, $r = 3$, in order to minimize the spatial error over the uniform spatial mesh $\mathcal{T}_h$ of mesh size $h = 0.0625$. We then compute the temporal experimental order of convergence by performing two different realizations with the time step lengths k_1 and k_2 and computing

$$\text{Rate} := \frac{\log(e(\cdot\,; h, k_1)) - \log(e(\cdot\,; h, k_2))}{\log(k_1) - \log(k_2)}.$$

The results, given in Table 2, confirm that our proposed numerical method (3.7) is of order two in time for both the wavefunction u and the potential v.

TABLE 2. Temporal experimental orders of convergence for u, v.

k	$e(u; k, h)$	Rate	$e(\mathsf{v}; k, h)$	Rate
0.04	3.72233e-4	-	9.60801e-4	-
0.02	9.49430e-5	1.971	2.51017e-4	1.936
0.01	2.39046e-5	1.990	6.41950e-5	1.967

5.2. **Discrete Conservation laws.** In this example, we investigate the behaviour of our numerical scheme (3.7) for system (1.2), with respect to the mass conservation (2.4) and energy balance (2.5) in two different cases: a) with constant coefficients $p(t)$ and $q(t)$ and b) with variable coefficients $p(t)$ and $q(t)$. We take $\Omega = (-1,1)^2$ which we discretize with linear finite elements over a uniform grid $\mathcal{T}_h$ consisting of squares with sides of length $h = 0.015625$. We take $\tau = 0$ and final time $T = 3$. We use $N = 3000$ time steps giving a time step length of $k = 10^{-3}$ and we choose $\alpha = \beta = 5$. The initial condition is taken to be

$$u(x,y,0) = \left(\sin(\frac{x}{\pi}) + i\cos(\frac{y}{\pi})\right)(1-x^2)(1-y^2), \tag{5.2}$$

which vanishes along the boundary of Ω ($\mu = 0$ in (1.1)).

5.2.1. *Constant Coefficients $p(t)$, $q(t)$.* In this case we take $p(t) = \frac{\varepsilon}{50}$, $q(t) = \frac{1}{\varepsilon}, \forall t$ and we expect that both mass and energy are conserved at the discrete level. We allow ε to vary in order to analyze how this affects the errors in the conservation laws. We then compute the global conservation law errors (3.10), (3.17), given by

$$\mathcal{M}_e^n := \left|\mathcal{M}_h^n - \mathcal{M}_h^0\right|, \tag{5.3}$$

$$\mathcal{E}_{e,gl}^n := \left| \left(p\mathcal{E}_{k,h}^n + \frac{q}{2}(2\mathcal{E}_{\mathsf{v}_2,h}^n - \mathcal{E}_{\mathsf{v}_1,h}^n)\right) - \left(p\mathcal{E}_{k,h}^1 + \frac{q}{2}(2\mathcal{E}_{\mathsf{v}_2,h}^1 - \mathcal{E}_{\mathsf{v}_1,h}^1)\right)\right|. \tag{5.4}$$

(Note that this definition of global energy error only applies to constant coefficients.) From Table 3, we observe that the density and the energy are conserved to double precision accuracy for all values of ε as expected. *Note that each row is roughly 1000 time-steps after the previous one.*

TABLE 3. Errors in the conservation laws : $p(t)$, $q(t)$ constant

	$\varepsilon = 1$		$\varepsilon = 0.1$		$\varepsilon = 0.01$	
t_n	$\mathcal{M}_e^n$	$\mathcal{E}_{e,gl}^n$	$\mathcal{M}_e^n$	$\mathcal{E}_{e,gl}^n$	$\mathcal{M}_e^n$	$\mathcal{E}_{e,gl}^n$
0	4.55e-15	2.39e-16	7.22e-16	2.58e-15	3.94e-15	9.57e-15
1	2.06e-14	3.29e-16	4.11e-15	1.39e-15	3.55e-15	1.60e-14
2	4.33e-14	1.75e-16	1.66e-15	2.36e-15	8.55e-15	1.54e-14
3	5.97e-14	3.03e-16	7.32e-15	2.01e-15	1.44e-14	2.56e-14

5.2.2. *Variable Coefficients $p(t)$, $q(t)$.* For the variable coefficient case we take $p(t) = \frac{\varepsilon}{50}t$, $q(t) = \frac{1}{\varepsilon}t^{\frac{1}{2}}, \forall t$. Here we have to introduce the local error for the discrete energy balance law, namely

$$\begin{aligned}\mathcal{E}_{e,loc}^n := \Bigg| &\left(p(t_{n-1/2})\mathcal{E}_{k,h}^n - \frac{q(t_{n-1/2})}{2}\left(2\mathcal{E}_{\mathsf{v}_2,h}^n - \mathcal{E}_{\mathsf{v}_1,h}^n\right)\right) - \\ &\left(p(t_{n-3/2})\mathcal{E}_{k,h}^{n-1} - \frac{q(t_{n-3/2})}{2}\left(2\mathcal{E}_{\mathsf{v}_2,h}^{n-1} - \mathcal{E}_{\mathsf{v}_1,h}^{n-1}\right)\right)\Bigg|.\end{aligned} \tag{5.5}$$

Table 4 shows the corresponding conservation of mass (3.10) and balance of energy (3.15). We observed that both are recovered to double precision of accuracy for all values of ε.

TABLE 4. Errors in the conservation laws : variable $p(t)$, $q(t)$

	$\varepsilon = 1$		$\varepsilon = 0.1$		$\varepsilon = 0.01$	
t_n	$\mathcal{M}_e^n$	$\mathcal{E}_{e,loc}^n$	$\mathcal{M}_e^n$	$\mathcal{E}_{e,loc}^n$	$\mathcal{M}_e^n$	$\mathcal{E}_{e,loc}^n$
0	2.05e-15	6.69e-16	4.49e-15	6.27e-15	6.55e-15	1.08e-15
1	1.91e-14	5.81e-16	9.81e-15	3.29e-15	5.55e-15	1.74e-14
2	5.73e-14	3.62e-16	1.97e-14	4.02e-15	8.91e-15	2.86e-14
3	9.38e-14	2.71e-16	1.47e-13	4.39e-15	1.78e-14	4.39e-14

5.3. **Variable time-step k_n.** We examine now the effect of variable time-step in the mass conservation (2.4) and energy balance (2.5) of system (1.2). We take (5.2) as an initial condition, $\alpha = \beta = 5$ and $\epsilon = 0.01$. The domain $\Omega = (-1, 1)^2$ is discretized by a uniform grid $\mathcal{T}_h$ consisting of squares with sides of length $h = 0.015625$, and we consider cubic finite elements on $\mathcal{T}_h$ resulting a spatial discretization error which is almost negligible. We take $\tau = 0$ and final time $T = 3$. We split the time interval $[0, T] = \cup_{j=1}^{12}[T_{j-1}, T_j]$ with $T_j = j/4,\ 0 \leq j \leq 12$. In each subinterval $[T_{j-1}, T_j)$ we use a different time step $k_j = j \cdot 1.25e-03,\ 1 \leq j \leq 12$. We monitor the error in discrete mass conservation (3.10) by means of $\mathcal{M}_e^j$ which was defined in (5.3). Moreover we monitor error in the energy balance law (3.17) by means of the global error $\mathcal{E}_{e,gl}^j$ defined in (5.4), and of the local error $\mathcal{E}_{e,loc}^j$ defined in (5.5).

At this point one should also recall that, according to Proposition 3.3, the size of $\mathcal{E}_{e,loc}^j$ at the points of change of time-step size is expected to be equal to the residual

$$\mathcal{R}^j := \left| \frac{q(t_{j-1/2})}{4} \frac{k_{j-1} - k_j}{k_{j-1} + k_j} k_j^2 \|\bar{\partial} \nabla V_h^{j-1/2}\|^2 \right|. \tag{5.6}$$

Table 5. Errors in the conservation laws : variable time-step

T_j	k_j	k_{j+1}	$\mathcal{M}_e^j$	$\mathcal{E}_{e,gl}^j$	$\mathcal{E}_{e,loc}^j$	$\mathcal{R}^j$
0.25	1.250e-03	2.500e-03	2.99e-15	3.11e-15	2.88e-11	1.28e-11
0.50	2.500e-03	3.750e-03	7.54e-14	2.93e-11	1.92e-10	1.22e-10
0.75	3.750e-03	5.000e-03	9.30e-14	2.21e-10	6.09e-10	4.42e-10
1.00	5.000e-03	6.250e-03	1.07e-13	8.31e-10	1.40e-09	1.09e-09
1.25	6.250e-03	7.500e-03	1.23e-13	2.23e-09	2.69e-09	2.20e-09
1.50	7.500e-03	8.750e-03	1.28e-13	4.92e-09	4.66e-09	3.92e-09
1.75	8.750e-03	1.000e-02	1.39e-13	9.59e-09	7.37e-09	6.32e-09
2.00	1.000e-02	1.125e-02	1.41e-13	1.70e-08	1.10e-08	9.71e-09
2.25	1.125e-02	1.250e-02	1.49e-13	2.80e-08	1.61e-08	1.42e-08
2.50	1.250e-02	1.375e-02	1.53e-13	4.40e-08	2.24e-08	2.00e-08
2.75	1.375e-02	1.500e-02	1.59e-13	6.64e-08	3.04e-08	2.72e-08
3.00	1.500e-02	–	1.63e-13	9.68e-08	–	–

Our findings are presented in Table 5. Each row $j,\ 1 \leq j \leq 12$ corresponds to the time interval $[T_{j-1}, T_j)$ and T_j is printed in the first column, while the corresponding time-step k_j is shown in the second column. The time-step size changes right after T_j; for the computation of the numerical solution in $[T_j, T_{j+1})$ with new time-step k_{j+1} appears (cf. equation (3.2)); this k_{j+1} is printed in the third column. The global mass error at T_j is printed in the fourth column, and the global energy error at T_j is printed in the fifth column. The local error in energy due to the change of time-step size around T_j is printed in the sixth column. The predicted residual, which is expected to be equal to the local energy error, is printed in the last column. We observe that conservation of mass is essentially unaffected by the time-step change while the energy loss in monitored accurately by the residual derived in Proposition 3.3. We note that, during this computation the time-step changed 11 times and grew by a factor of 20.

5.4. **A cosmological example.** One application of the Schrödinger-Poisson system (1.1) comes from the field of cosmology. Indeed, the d-dimensional Schrödinger-Poisson system (1.1) can be used as an approximation to the computationally expensive $2d$-dimensional Vlasov-Poisson system used to describe collisionless self-gravitating matter [35]. For this numerical experiment, we proceed as in [35]. Firstly, we take $\mu = \|u_0\|^2 = 1$ and periodic boundary conditions in (1.1). The initial time is $\tau = 0.01$ and the final time $T = 0.088$. Time dependent coefficients are used, namely $p(t) = \frac{\varepsilon}{2t^{3/2}}$,

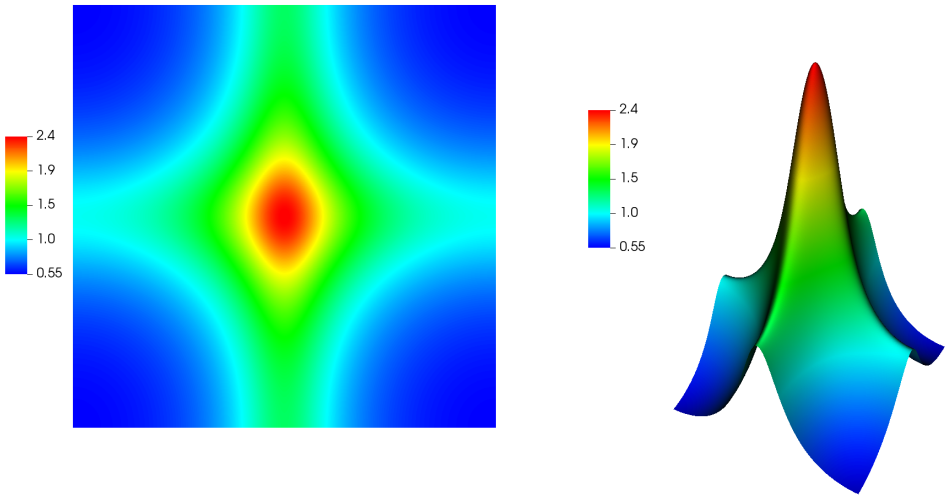

FIGURE 1. The initial density $|u_0|^2$ used in (5.7).

$q(t) = \frac{\beta}{\varepsilon t^{1/2}}$, where $\beta = 1.5$ and $\varepsilon = 6e-5$. Thus our cosmological example reads as

$$
\begin{cases}
u_t - \dfrac{\mathrm{i}\varepsilon}{2t^{3/2}}\Delta u + \dfrac{\mathrm{i}\beta}{\varepsilon t^{1/2}}\mathsf{v}u = 0, & \text{in } \Omega\times(\tau,T),\\
\Delta \mathsf{v} = |u|^2 - 1, & \text{in } \Omega\times(\tau,T),\\
u(\mathbf{x},0) = u_0(\mathbf{x}), & \text{in } \Omega,\\
\|u_0\|_{L^2}^2 = 1 : u, \mathsf{v} \text{ periodic} & \text{on } \partial\Omega\times(\tau,T).
\end{cases} \tag{5.7}
$$

This problem is a special case of system (1.1), and therefore satisfies the mass conservation (2.4) and the energy balance (2.5), which for the particular $p(t)$ and $q(t)$ takes the form:

$$
\frac{\varepsilon}{2t^{3/2}}\frac{\mathrm{d}}{\mathrm{d}t}\mathcal{E}_k(t) + \frac{\beta}{\varepsilon t^{1/2}}\frac{\mathrm{d}}{\mathrm{d}t}\left(2\mathcal{E}_{\mathsf{v}_2}(t) - \mathcal{E}_{\mathsf{v}_1}(t)\right) = 0 \implies \frac{\varepsilon^2}{2}\frac{\mathrm{d}}{\mathrm{d}t}\mathcal{E}_k(t) + t\beta\frac{\mathrm{d}}{\mathrm{d}t}\left(2\mathcal{E}_{\mathsf{v}_2}(t) - \mathcal{E}_{\mathsf{v}_1}(t)\right) = 0.
$$

The fully discrete relaxation scheme (3.2) with constant time-step $k_n = k,\ \forall n$ for (5.7) is

$$
\begin{cases}
\overline{\partial} U_h^n - \dfrac{\mathrm{i}\varepsilon}{2t_{n-1/2}^{3/2}}\Delta_h^n U_h^{n-1/2} + \dfrac{\mathrm{i}\beta}{\varepsilon t_{n-1/2}^{1/2}}\mathcal{P}_h^n\left(V_h^{n-1/2}U_h^{n-1/2}\right) = 0,\\
\Delta_h^n V_h^{n-1/2} = \Phi_h^{n-1/2},\\
\Phi_h^{n-1/2} = 2\mathcal{P}_h^n(|U_h^{n-1}|^2 - 1) - \Phi_h^{n-3/2}.
\end{cases} \tag{5.8}
$$

Scheme (5.8) satisfies the discrete mass conservation (3.10) and the local discrete energy balance (3.15), which for the particular $p(t)$ and $q(t)$ takes the form:

$$
\varepsilon^2\overline{\partial}(\|\nabla U_h^n\|^2) + \beta t_{n-1/2}\left(\overline{\partial}(\|\nabla V_h^{n-1/2}\|^2) + 2\int_\Omega \overline{\partial}(V_h^{n-1/2}(|U_h^n|^2 - \mu))\,\mathrm{d}x\right) = 0, \forall n. \tag{5.9}
$$

We now consider the benchmark case of a *sine wave collapse*. The initial condition is as given in [35] and its position density is displayed in Figure 1. The domain Ω is discretized with linear finite elements over one of two different uniform grids: a 1024×1024 and a 2048×2048 grid while the time domain (τ, T) is discretized using 1560 uniform time steps yielding a time step size of $k = 5e-5$. Results of the numerical simulations are shown in Figure 2. For comparison purposes, we plot the density $|U_h(t_n)|^2$ at three different time instances ($t_n = 0.023,\ 0.033,\ 0.088$) all of which are in excellent agreement with the plots in [35].

Due to the small value of ε, the wavefunction is highly oscilliatory which can be readily seen in the 1024×1024 grid but is much more apparent in the 2048×2048 grid. We thus postprocess the

density by applying a Gaussian filter of width $\sigma = 0.0035$ which eliminates spurious oscillations – this is shown in Figure 3 at the final time $\tau = T$ for both grids.

For this example, the density is conserved up to double precision while the energy is conserved to at least 8 digits of accuracy, see Table 6. The loss of accuracy in the energy balance is mainly due to the loss of periodicity for $\nabla \mathsf{v}$ at the discrete level. Indeed, the periodicity for wavefuction and potential is preserved at the discrete level, however it is lost for ∇V_h^n which is a crucial assumption in (3.20) for proving (3.16). We have computed the L^2-norm of the difference between the values of the $\nabla V_h^n,\ n = 1, \dots,$ along the corresponding horizontal and vertical boundaries of the domain and it is found to vary from $10^{-7} - 10^{-10}$ depending on the grid size.

TABLE 6. Mass conservation error(MCe) and Energy balance error (EBe)

Grid	512×512		1024×1024		2048×2048	
t	MCe	EBe	MCe	EBe	MCe	EBe
0.023	4.329e-15	1.222e-08	1.010e-13	9.039e-10	1.852e-13	1.131e-11
0.033	1.643e-14	2.427e-08	1.210e-13	9.675e-10	1.912e-13	2.323e-11
0.088	3.775e-14	5.065e-08	1.386e-13	9.273e-10	5.332e-13	6.037e-11

ACKNOWLEDGEMENTS

The authors acknowledge the support from the Carnegie Trust Research Incentive Grant RIG008215. I.K. would also like to acknowledge the support from London Mathematical Society through an Emmy Noether Fellowship. In addition, Th. K. and I.K. thank the Edinburgh Mathematical Society for the Covid Recovery Fund that allowed for the completion and the submission of this paper. Moreover, the authors would like to express their gratitude to Dr. K. Vattis, Prof. C. Skordis and especially Dr. M. Kopp for their valuable help and support in setting up the cosmological example reported in Section 5. Finally, the authors would like to thank the anonymous reviewers for their valuable comments and suggestions.

REFERENCES

[1] N.B. Abdallah, F. Méhats, O. Pinaud, *On an open transient Schrödinger-Poisson system*, Math. Models Methods Appl. Sci. **15**, 667–688, 2005.

[2] G. Akrivis, V. Dougalis, O. Karakashian, *On fully discrete Galerkin methods of second-order temporal accuracy for the nonlinear Schrödinger equation*, Numer. Math. **59**, 31-53, 1991.

[3] G.D. Akrivis, V.A. Dougalis, O.A. Karakashian, W.R. McKinney, *Numerical approximation of blow-up of radially symmetric solutions of the nonlinear Schrödinger equation*, SIAM J. Sci. Comput. **25**, 186–212, 2003.

[4] G. Akrivis, D. Li, *Structure-preserving Gauss methods for the nonlinear Schrödinger equation*, Calcolo **58**, 1–25, 2021.

[5] E. Arriola, J. Soler, *A variational approach to the Schrödinger-Poisson System: Asymptotic behaviour, breathers, and stability*, J. Stat. Phys. **103**, 1069–1106, 2001.

[6] W. Auzinger, T. Kassebacher, O. Koch, M. Thalhammer, *Convergence of a Strang splitting finite element discretization for the Schrödinger-Poisson equation*, ESAIM Math. Model. Numer. Anal. **51**, 1245–1278, 2017.

[7] W. Bao, D. Jaksch, P.A. Markowich, *Numerical solution of the Gross-Pitaevskii equation for Bose-Einstein condensation*, J. Comput. Phys. **187**, 318–342, 2003.

[8] W. Bangerth, R. Hartmann, G. Kanschat, `deal.II` – *A general-purpose object-oriented finite element library*, ACM Transactions on Mathematical Software, 33(4), article 24, 2007.

[9] W. Bao, N. Mauser, H.P. Stimming, *Effective one particle quantum dynamics of electrons: A numerical study of the Schrödinger-Poisson-Xα model*, Comm. Math. Sciences **1**, 809–828, 2003.

[10] Ch. Besse, *A relaxation scheme for the nonlinear Schrödinger equation*, SIAM J. Numer. Anal. **42**, 934–952, 2004.

[11] Ch. Besse, S. Descombes, G. Dujardin, I. Lacroix-Violet, *Energy-preserving methods for nonlinear Schrödinger equations*, IMA J. Numer. Anal. **41**, 618–653, 2021.

[12] C. Besse, G. Dujardin, I. Lacroix-Violet, *High order exponential integrators for nonlinear Schrödinger equations with application to rotating Bose–Einstein condensates*, SIAM J. Numer. Anal. **55**, 1387–1411, 2017.

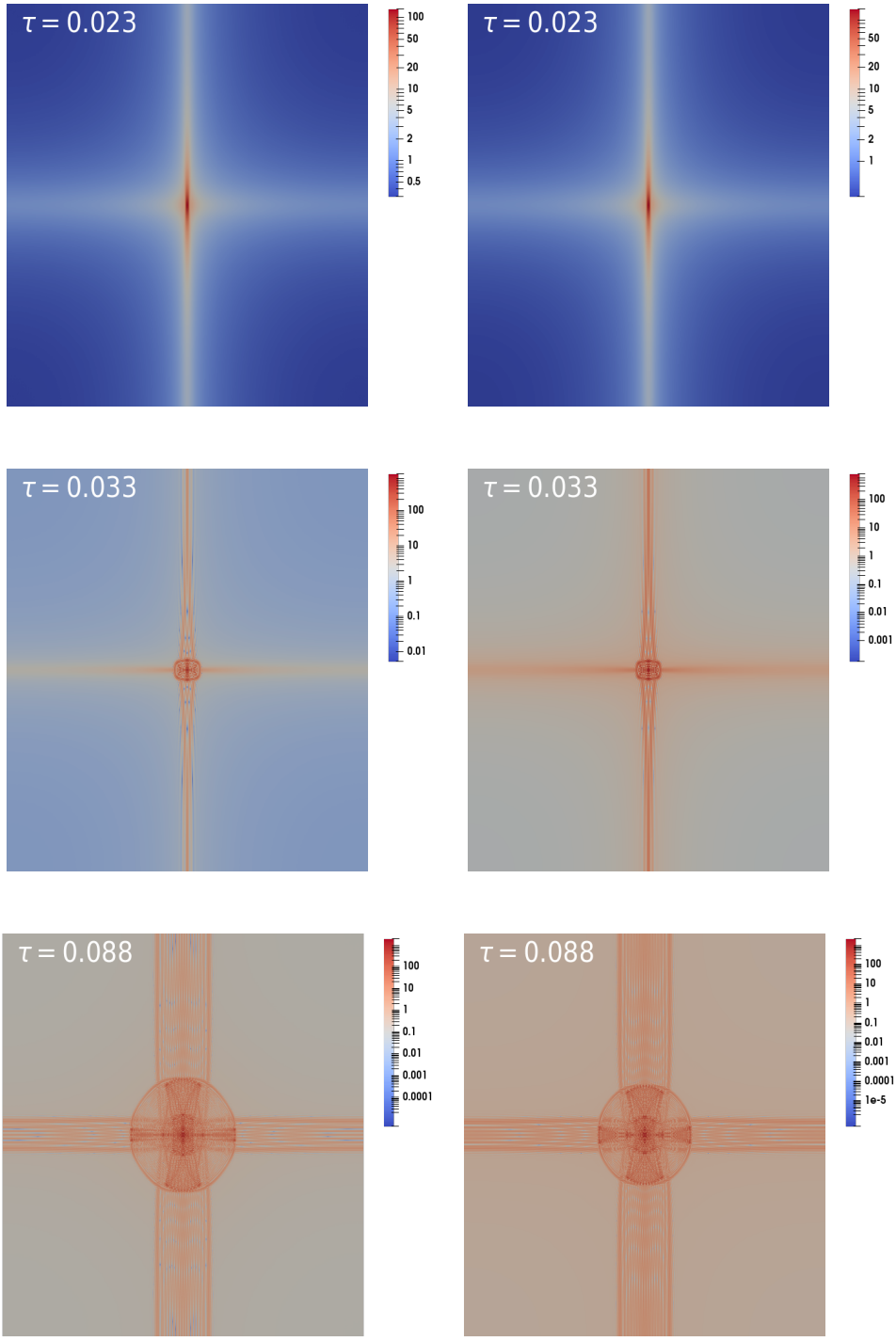

FIGURE 2. The density $|U_h(t)|^2$ (logarithmic scale) at $t = 0.023,\ 0.033,\ 0.088$: 1024×1024 grid (left), 2048×2048 grid (right).

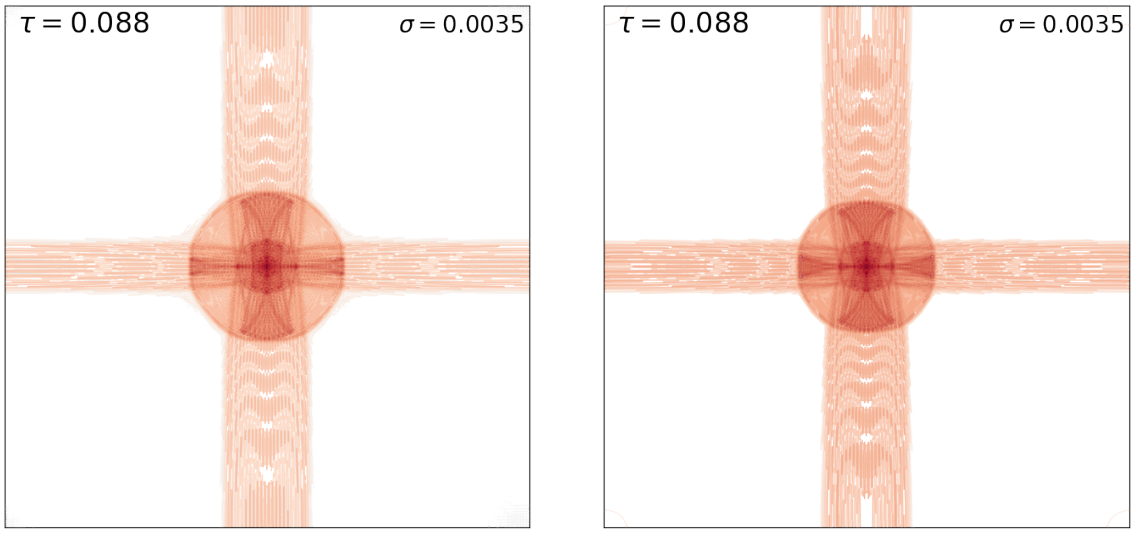

FIGURE 3. The density $|U_h(t)|^2$ (logarithmic scale) at $t = T$ with Gaussian filtering of width $\sigma = 0.0035$: 1024×1024 grid (left), 2048×2048 grid (right).

[13] C. Bardos, L. Erdös, F. Golse, N. Mauser, H-T Yau, *Derivation of the Schrödinger-Poisson equation from the quantum N-body problem*, C. R. Acad. Sci. Paris, Ser. I **334**, 515-520, 2002.
[14] H. Berland, A.L. Islas, C.M. Schober, *Conservation of phase space properties using exponential integrators on the cubic Schrödinger equation*, J. Comput. Phys. **225**, 284–299, 2007.
[15] P. Bertrand, N. Van Tuan, M. Gros, B. Izrar, M. Feix, J. Gutierrez, *Classical Vlasov plasma description through quantum numerical methods*, J. Plasma Phys. **23**, 401-422, 1980.
[16] S. Bohun, R. Illner, H. Lange, P.F Zweifel, *Error estimates for Galerkin approximations to the periodic Schrödinger-Poisson system*, ZAMM Journal of applied mathematics and mechanics/ Zeitschrift für angewandte Mathematik und Mechanik **76**, 7–13, 1996
[17] F. Brezzi, P.A. Markowich, *The three-dimensional Wigner-Poisson problem: Existence, uniqueness and approximation*, Math. Methods Appl. Sci. **14**, 35–61, 1991
[18] F. Castella, *L^2-solutions to the Schrödinger-Poisson system: existence, uniqueness, time behaviour and smoothing effects*, Math. Mod. Meth. Appl. Sci. **7**, 1051-1083, 1997.
[19] T. Cazenave, *Semilinear Schrodinger Equations* (Vol. 10). American Mathematical Soc. 2003.
[20] P. Chartier, N.J. Mauser, F. Méhats, Y. Zhang, Y., *Solving highly-oscillatory NLS with SAM: numerical efficiency and long-time behavior*, Discrete Contin. Dyn. Syst.-S **9**, 1327, 2016.
[21] G. Davies, L. Widrow, *Test-bed simulations of collisionless, self-gravitating systems using the Schrödinger method*, The Astrophysical Journal **485**, 484, 1997.
[22] M. Delfour, M. Fortin, G. Payr, *Finite-difference solutions of a non-linear Schrödinger equation*, J. Comput. Phys. **44**, 277–288, 1981.
[23] M. Dehghan, V. Mohammadi, *A numerical scheme based on radial basis function finite difference (RBF-FD) technique for solving the high-dimensional nonlinear Schrödinger equations using an explicit time discretization: Runge-Kutta method*, Comput. Phys. Commun. **217**, 23–34, 2017.
[24] M. Dehghan, A. Taleei, *A compact split-step finite difference method for solving the nonlinear Schrödinger equations with constant and variable coefficients*, Comput. Phys. Commun. **181**, 43–51, 2010.
[25] M. Ehrhardt, A. Zisowsky, *Fast calculation of energy and mass preserving solutions of Schrödinger-Poisson systems on unbounded domains*, J. Comput. Appl. Math. **187**, 1-28, 2006.
[26] Z. Fei, V.M. Pérez-García, L. Vázquez, *Numerical simulation of nonlinear Schrödinger systems: a new conservative scheme* Appl. Math. Comput. **71**, 165–177, 1995.
[27] M. Hederi, A.L. Islas, K. Reger, C.M. Schober, *Efficiency of exponential time differencing schemes for nonlinear Schrödinger equations*, Math. Comput. Simul. **127**, 101–113, 2016.
[28] M. Ilati, M. Dehghan, *DMLPG method for numerical simulation of soliton collisions in multi-dimensional coupled damped nonlinear Schrödinger system which arises from Bose-Einstein condensates*, Appl. Math. Comput. **346**, 244–253, 2019.
[29] R. Illner, P.F. Zweifel, H. Lange, *Global existence, uniqueness and asymptotic behaviour of solutions of the Wigner-Poisson and Schrödinger-Poisson systems*, Math. Meth. Appl. Sci. **17**, 349–376, 1994.
[30] S. Jin , H. Wu, X. Yang, *A numerical study of the Gaussian beam methods for Schrödinger-Poisson equations*, J. Comput. Appl. Math. **28**, 261-272, 2010.

[31] M. Karner, A. Gehring, S. Holzer, M. Pourfath, M. Wagner, W. Goes, M. Vasicek, O. Baumgartner, C. Kernstock, K. Schnass, G. Zeiler, *A multi-purpose Schrödinger-Poisson solver for TCAD applications* J. Comput. Electron. **6**, 179–182, 2007.
[32] O. Karakashian, Ch. Makridakis, *A space-time finite element method for the nonlinear Schrödinger equation: the discontinuous Galerkin method*, Math. Comp. **67**, 479–499, 1998.
[33] O. Karakashian, Ch. Makridakis, *A space-time finite element method for the nonlinear Schrödinger equation: the continuous Galerkin method*, SIAM J. Numer. Anal. **36**, 1779–1807, 1999.
[34] Th. Katsaounis, I. Kyza, *A posteriori error analysis for evolution nonlinear Schrödinger equations up to the critical exponent*, SIAM J. Numer. Anal. **56**, 1405–1434, 2018.
[35] M. Kopp, K. Vattis, C. Skordis, *Solving the Vlasov equation in two spatial dimensions with the Schrödinger method*, Phys. Rev. D **96**, 123532, 2017.
[36] T. Lu, W. Cai, *A Fourier spectral-discontinuous Galerkin method for time-dependent 3-D Schrödinger-Poisson equations with discontinuous potentials*, J. Comput. Appl. Math. **220**, 588-614, 2008.
[37] C. Lubich, *On splitting methods for Schrödinger-Poisson and cubic nonlinear Schrödinger equations*, Math. Comp. **77**, 2141–2153, 2008.
[38] P. Markowich, C. Ringhofer, C. Schmeiser, *Semiconductor equations*, Springer, Berlin, 1990.
[39] A. Paredes, D.N. Olivieri, H. Michinel, *From optics to dark matter: A review on nonlinear Schrödinger-Poisson systems* Physica D: Nonlinear Phenomena **403**, 132301, 2020.
[40] C. Ringhofer, J. Soler, *Discrete Schrödinger-Poisson systems preserving energy and mass*, Appl. Math. Lett. **13**, 27–32, 2000.
[41] P.K. Shukla, B. Eliasson, *Colloquium: Nonlinear collective interactions in quantum plasmas with degenerate electron fluids*, Rev. Mod. Phys. **83**, 885, 2011.
[42] M. Thalhammer, *Convergence analysis of high-order time-splitting pseudo-spectral methods for nonlinear Schrödinger equations*, SIAM J. Numer. Anal. **50**, 3231–3258, 2012.
[43] P. Tod, I.M. Moroz, *An analytical approach to the Schrödinger-Newton equations*, Nonlinearity **12**, 201–216, 1999.
[44] C. Uhlemann, M. Kopp, and T. Haugg, *Schrödinger method as N-body double and UV completion of dust*, Phys. Rev. D **90**, 023517, 2014.
[45] L. Widrow, N. Kaiser, *Using the Schrödinger equation to simulate collisionless matter*, Astrophys. J. Lett. **416**, L71, 1993.
[46] Y. Zhang and X. Dong, *On the computation of ground state and dynamics of Schrödinger-Poisson-Slater system*, J. Comput. Phys. **230**, 2660–2676, 2011.
[47] Y. Zhang, *Optimal error estimates of compact finite difference discretizations for the Schrödinger-Poisson system*, Commun. Commut. Phys. **13**, 1357–1388, 2015.
[48] P. Zhang, Y. Zheng, N. Mauser, *The limit from the Schrödinger-Poisson to the Vlasov-Poisson equations with general data in one dimension*, Comm. Pure Appl. Math.**55**, 582–632, 2002.
[49] G. Zouraris, *On the convergence of a linear two-step finite element method for the nonlinear Schrödinger equation*, M2AN Math. Model. Numer. Anal. **35**, 389–405, 2001.
[50] G.E. Zouraris, *Error estimations pf the Besse relaxation scheme for a semilinear heat equation*, ESAIM: Math. Model. Numer. Anal. **55** 301–328, 2021.

(Agissilaos Athanassoulis) Department of Mathematics, University of Dundee, Dundee DD1 4HN, Scotland, UK
Email address: a.athanassoulis@dundee.ac.uk

(Theodoros Katsaounis) Dept. of Math. and Applied Mathematics, Univ. of Crete, GREECE & IACM–FORTH, Heraklion, GREECE
Email address: thodoros.katsaounis@uoc.gr

(Irene Kyza) Department of Mathematics, University of Dundee, Dundee DD1 4HN, Scotland, UK
Email address: ikyza@dundee.ac.uk

(Stephen Metcalfe) Dept. of Mechanical Engineering, McGill Univ., Montreal, Canada
Email address: smetcalfephd@gmail.com